ACS central science

http://pubs.acs.org/journal/acscii

Research Article

Targeting the SARS-CoV-2 RNA Genome with Small Molecule Binders and Ribonuclease Targeting Chimera (RIBOTAC) Degraders

Hafeez S. Haniff,[#] Yuquan Tong,[#] Xiaohui Liu, Jonathan L. Chen, Blessy M. Suresh, Ryan J. Andrews, Jake M. Peterson, Collin A. O'Leary, Raphael I. Benhamou, Walter N. Moss, and Matthew D. Disney*

Cite This: https://dx.doi.org/10.1021/acscentsci.0c00984

Read Online

ACCESS | Metrics & More | Article Recommendations | Supporting Information

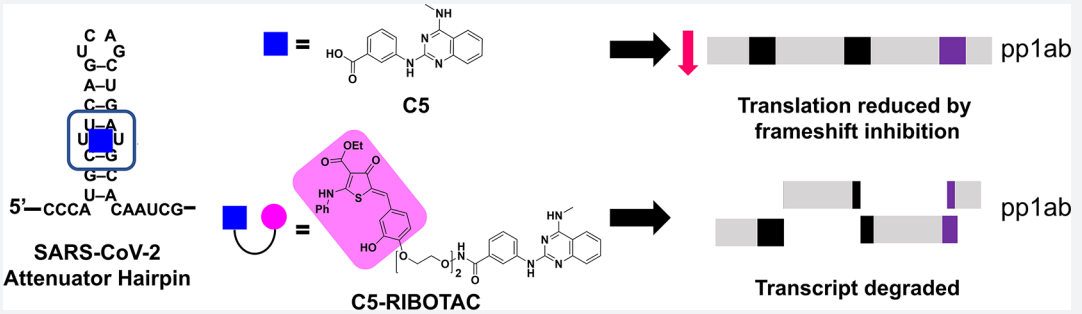

ABSTRACT: COVID-19 is a global pandemic, thus requiring multiple strategies to develop modalities against it. Herein, we designed multiple bioactive small molecules that target a functional structure within the SARS-CoV-2's RNA genome, the causative agent of COVID-19. An analysis to characterize the structure of the RNA genome provided a revised model of the SARS-CoV-2 frameshifting element, in particular its attenuator hairpin. By studying an RNA-focused small molecule collection, we identified a drug-like small molecule (**C5**) that avidly binds to the revised attenuator hairpin structure with a K_d of 11 nM. The compound stabilizes the hairpin's folded state and impairs frameshifting in cells. The ligand was further elaborated into a ribonuclease targeting chimera (RIBOTAC) to recruit a cellular ribonuclease to destroy the viral genome (**C5-RIBOTAC**) and into a covalent molecule (**C5-Chem-CLIP**) that validated direct target engagement and demonstrated its specificity for the viral RNA, as compared to highly expressed host mRNAs. The RIBOTAC lead optimization strategy improved the bioactivity of the compound at least 10-fold. Collectively, these studies demonstrate that the SARS-CoV-2 RNA genome should be considered druggable.

In late 2019, a respiratory illness was discovered in China that soon would cover the face of the globe. Severe acute respiratory syndrome (SARS)-CoV-2, the virus that causes COVID-19, has wreaked havoc on our healthcare systems, our economies, and our daily lives.[1,2] Shortly after its discovery, its genome was sequenced, and that sequence was deposited into public databases. Analysis revealed that the virus is a member of the coronaviridae family and shares many features with other strains.[3]

One option to combat the virus is the development of vaccines, with several candidates generated toward the SARS-CoV-2 spike protein.[4] Vaccines will not eliminate SARS-CoV-2, however, as not all susceptible in the population will be vaccinated. Moreover, this virus (and related coronaviruses) can persist within wildlife hosts, thus posing a threat of zoonotic transfer.[5] Therapeutics to treat an existing infection are therefore an urgent medical need. Remdesivir, a drug used to treat Ebola, has had success in COVID-19 patients and garnered fast-track FDA approval.[6,7] However, alternatives are needed, with particular interest in those that interrupt the virus' essential processes. Indeed, since the SARS-CoV-2 outbreak, many groups have pursued this strategy.[8,9] Here, we report targeting conserved, functional structures within SARS-CoV-2's genome with small molecules to inhibit one of the virus' essential processes, frameshifting.

Several groups have interrogated the structure of the SARS-CoV-2 RNA genome computationally and experimentally, identifying a convergence of structures in both coding and noncoding regions.[10−12] The structural elements within these regions could be novel targets for small molecule intervention.[13] Indeed, targeting functional structural elements within disease-associated RNAs affords bioactive small molecules,[14,15] including those within RNAs of viral origin such as SARS-CoV[16,17] and SARS-CoV-2.[18]

Of particular interest, sites of structural convergence were identified within the SARS-CoV-2 frameshifting element

Received: July 24, 2020

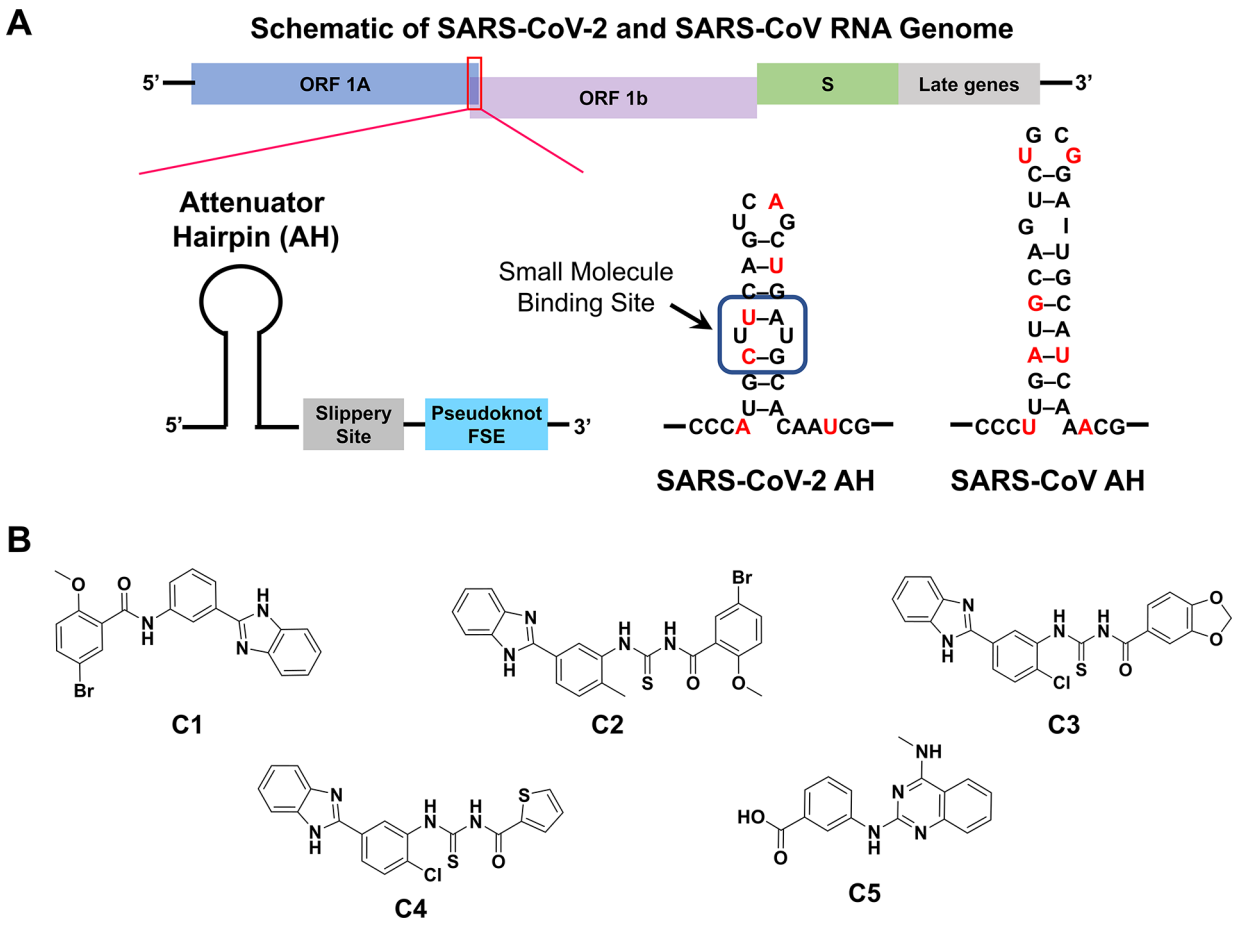

Figure 1. SARS-CoV-2's frameshifting element controls ORF translation. (A) Schematic of the SARS-CoV-2 and SARS-CoV RNA genome, encoding two open reading frames (ORFs), ORF 1a and ORF 1b. ORF 1b is out of frame with the ATG start codon of ORF 1a, and thus a frameshifting element (FSE) between the two ORFs is responsible for its translation. This element is comprised of an attenuator hairpin (AH), a slippery sequence, and a pseudoknot element that triggers a −1-frameshift, allowing translation of ORF 1b that encodes pp1a and pp1ab. The SARS-CoV-2 AH contains a 5′CUU/3′GUA internal loop, not found in the SARS-CoV AH, that can be targeted by a small molecule. Small molecule binding stabilizes the attenuator hairpin and inhibits frameshifting. (B) A microarray screen of an RNA-focused library (n = 3,271) identified five small molecules that bind dose dependently to a model of the SARS-CoV-2 attenuator hairpin in the presence of an equimolar amount of a SARS-CoV-2 mutant in which the loop was mutated to an AU pair.

(FSE), which controls translation of the pp1a and pp1ab polyproteins that are critical for viral replication and pathogenesis (Figure 1A).[19,20] The FSE comprises an attenuator hairpin (AH),[21] slippery site (SS), and a three stemmed pseudoknot[22] that collectively can pause the ribosome to initiate frameshifting, thereby altering the protein coding content of the mRNA.[23] Interestingly, enhancing the thermodynamic stability of the FSE impairs frameshifting efficiency.[17,24] An alternative way to inhibit frameshifting therefore would be the stabilization of the FSE afforded by the binding of structure-specific ligands, which has been shown to be effective with other viral FSEs.[25] Herein, we have designed small molecules that inhibit SARS-CoV-2 frameshifting by two different modes of action: simple binding and degrading the viral genome by recruiting an endogenous nuclease that functions in the viral immune response.

RESULTS AND DISCUSSION

Small Molecule Microarray Screening to Identify Selective Binders to the SARS-CoV-2 Frameshift Attenuator Hairpin. A previous structural analysis of the SARS-CoV-2 FSE showed that the AH harbors a 1 × 1 nucleotide UU internal loop in its stem,[12] in contrast to the two bulges formed in the stem of the SARS-CoV AH and in a previous model of the SARS-CoV-2 AH[18] (Figures 1A and S1A). This internal loop motif was conserved in two models generated from computational analysis that combines free energy minimization and evolutionary conservation (ScanFold[12] and RNAz[11]) and is consistent with structural mapping data (DMS-MaPseq) of the SARS-CoV-2 genome in infected cells.[23] The conservation of this motif across these independent studies indicates the UU loop is indeed a *bona fide* structure, the binding of which could inhibit FSE function.

Thus, to identify novel small molecule binders, we studied the binding capacity of a 3,271-member RNA-focused compound collection, constructed by using the physiochemical properties of all known ligands that bind RNA and procured from commercial sources. The RNA-binding ligand data set is housed in the Inforna database, a catalog of experimentally determined RNA fold-small molecule interactions identified by our laboratory as well as those reported by others in the literature.[26,27] Chemotypes represented within the RNA-focused library include benzimidazoles, *bis*-benzimidazoles, guanidino-thiazoles, diaminopyrimidines, and 2,4-diaminoquinazolines. To study the binding of small molecules to the SARS-CoV-2 AH (Figure 1A), we constructed microarrays via

https://dx.doi.org/10.1021/acscentsci.0c00984
ACS Cent. Sci. XXXX, XXX, XXX−XXX

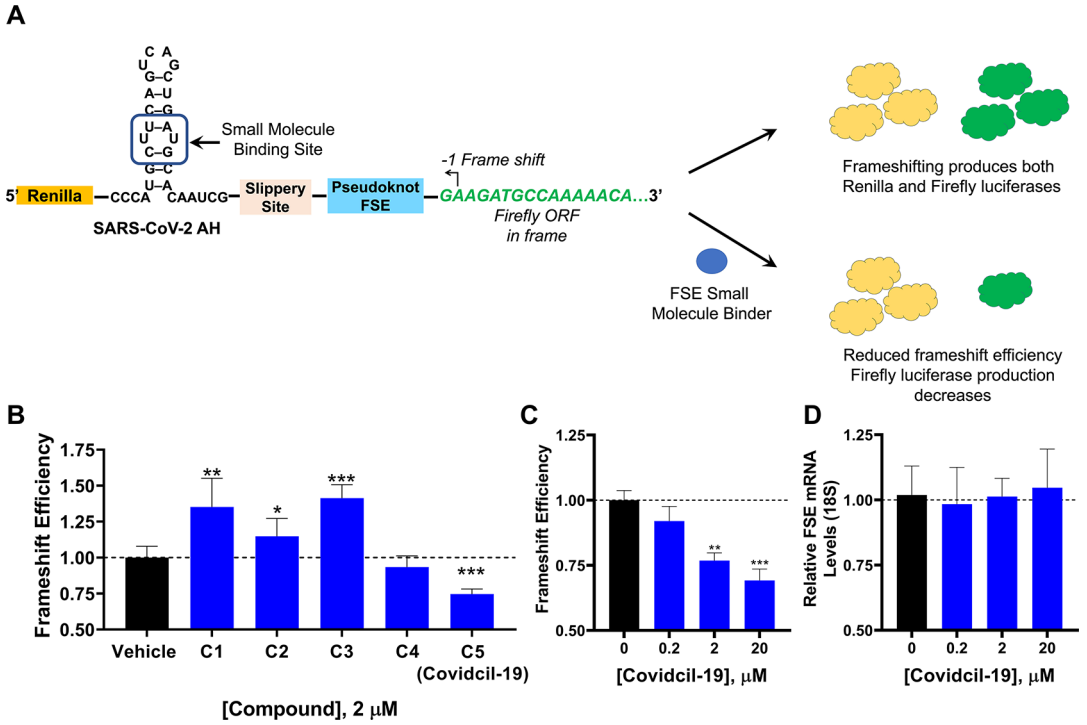

Figure 2. C5 reduces frameshifting efficiency of the SARS-CoV-2 FSE. (A) Schematic of a frameshifting reporter system in which an FSE is inserted upstream of two ORFs encoding Renilla (in-frame) and firefly luciferase (requires a −1 frameshift). In the absence of a small molecule binder, frameshifting occurs, producing both Renilla and firefly luciferase. Small molecule binding to the AH can inhibit frameshifting, reducing translation of firefly luciferase. (B) Effect of small molecules (2 μM) on SARS-CoV-2 frameshifting efficiency in HEK293T cells. Frameshifting efficiency is calculated by comparing the ratio of firefly luciferase activity: Renilla luciferase activity from the construct containing the FSE vs the construct without the FSE but with firefly luciferase in-frame (control ORF construct) (n = 8 for **C1**, **C2**, **C3**, and **C5**; n = 3 for **C4**). (C) **C5** dose dependently inhibits frameshifting. Frameshifting efficiency was calculated as described in panel B (n = 5). (D) Effect of **C5** on SARS-CoV-2 FSE RNA, as determined by RT-qPCR (n = 4). Data are reported as the mean ± S.E.M. P-values in panel B were calculated using a two-tailed Student t test, while p-values in panel C were calculated with a one-way ANOVA with multiple comparisons, where *, $p < 0.05$; **, $p < 0.01$; and ***, $p < 0.001$.

AbsorbArray, an approach that does not require covalent attachment of the compounds onto the array surface (i.e., site-specific immobilization).[28] In brief, small molecules are absorbed onto agarose-coated slides, washed, and then incubated with a labeled RNA, whether a single target of interest or a library of RNA motifs.[28] Thus, molecules in AbsorbArray should bind similarly to the RNA target whether on the array surface or in solution, with a potential trade-off that compounds with poor absorption may be washed away untested.

Using AbsorbArray, we identified 26 binders to SARS-CoV-2-AH (0.8% hit rate; Figure S1B). These initial hits can be classified into three major scaffolds: phenyl benzimidazoles (n = 11), phenyl thioureas (n = 6), and 2,4-diaminoquinazolines (n = 7), with two compounds not falling into any of these three categories. The 26 hits were further triaged by competitive screening in which the small molecules were arrayed in dose response and incubated with equimolar amounts of radioactively labeled (wild type) SARS-CoV-2-AH and unlabeled mutant SARS-CoV-2-AH, in which the 1 × 1 nucleotide UU internal loop was replaced with an AU base pair (Figure S1B). This competitive screening afforded five hits (**C1**−**C5**; Figures 1B and S1B) that were further investigated *in vitro* and in cells. Interestingly, many of the phenyl benzimidazoles and quinazolines no longer bound in the secondary assay, as three of the five compounds that progressed were phenyl thioureas (**C3**, **C4**, and **C5**).

Small Molecules Reduce Frameshifting Efficiency in Cells. To identify which of the five binding compounds affect the frameshifting efficiency of the SARS-CoV-2-FSE, we employed a Renilla-firefly luciferase reporter system transfected into HEK293T cells (Figure 2A). In the absence of the FSE, firefly luciferase is out of frame, and only Renilla luciferase is translated. Inserting the SARS-CoV-2 FSE upstream of the coding region allows a −1 frameshift to occur, producing both firefly and Renilla luciferases. Here, in HEK293T cells, the frameshifting efficiencies of the SARS-CoV-2 and SARS-CoV were both ∼40%, similar to previously observed percentages.[18] We hypothesized that ligand binding to the AH harbored in the FSE would stabilize its structure, reducing its ability to frameshift and hence generate firefly luciferase (Figure 2A).

We first studied the effect of 2 μM of **C1**−**C5** on frameshifting. Frameshifting efficiency was calculated by comparing the ratio of firefly and Renilla luciferase activities upon treatment of HEK293T cells expressing the SARS-CoV-2 FSE constructs to the ratio of firefly and Renilla luciferase activities upon treatment of HEK293T cells expressing a control construct lacking an FSE, as previously described.[18] Treated samples were then normalized to vehicle-treated samples. Only **C5** significantly decreased frameshifting efficiency, by 25 ± 1% (Figure 2B) and did so dose-dependently (Figure 2C). Importantly, this compound exhibited no toxicity at all concentrations tested, including

https://dx.doi.org/10.1021/acscentsci.0c00984
ACS Cent. Sci. XXXX, XXX, XXX−XXX

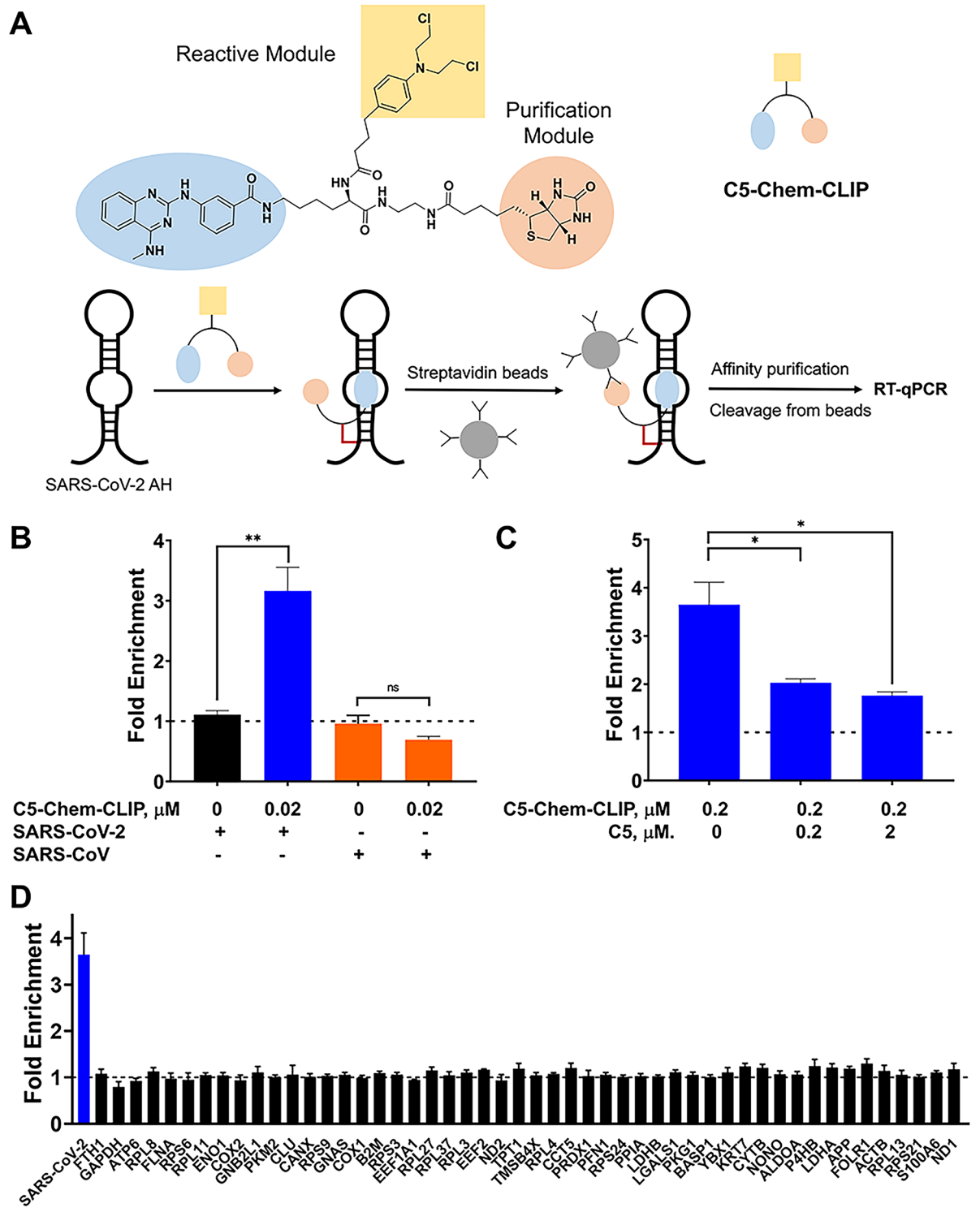

Figure 3. C5-Chem-CLIP, a covalent small molecule, directly engages the SARS-CoV-2 FSE, validating **C5**'s target site. (A) Top, Chemical structure of **C5-Chem-CLIP**, where compound **C5** was equipped with a chlorambucil cross-linking module and a biotin handle for pull-down. Cross-linking is proximity-based, driven by the RNA-binding module. Bottom, Schematic of Chem-CLIP work-flow. (B) Direct target engagement of SARS-CoV-2 FSE by **C5-Chem-CLIP** in cells, as assessed by Chem-CLIP. Enrichment was calculated by comparing the levels of SARS-CoV-2 RNA in the pulled down fraction (relative to 18S rRNA) to the levels of the SARS-CoV-2 RNA in the starting lysate (relative to 18S rRNA), as determined by RT-qPCR (n = 4). **C5-Chem-CLIP** did not bind the SARS-CoV RNA in cells as this virus strain lacks the ligand binding site (n = 4). (C) Competitive (C−) Chem-CLIP studies of the SARS-CoV-2 RNA by cotreating cells with varying concentrations of **C5** and a constant concentration of **C5-Chem-CLIP** (0.2 μM) (n = 4). (D) Profiling of 50 abundant mRNAs in cells treated with **C5-Chem-CLIP**; no enrichment was observed for any of the mRNAs. Thus, **C5-Chem-CLIP** selectively enriches for the SARS-CoV-2 FSE. Data are reported as the mean ± SEM. All p-values were calculated using a two-tailed Student t test.

https://dx.doi.org/10.1021/acscentsci.0c00984
ACS Cent. Sci. XXXX, XXX, XXX−XXX

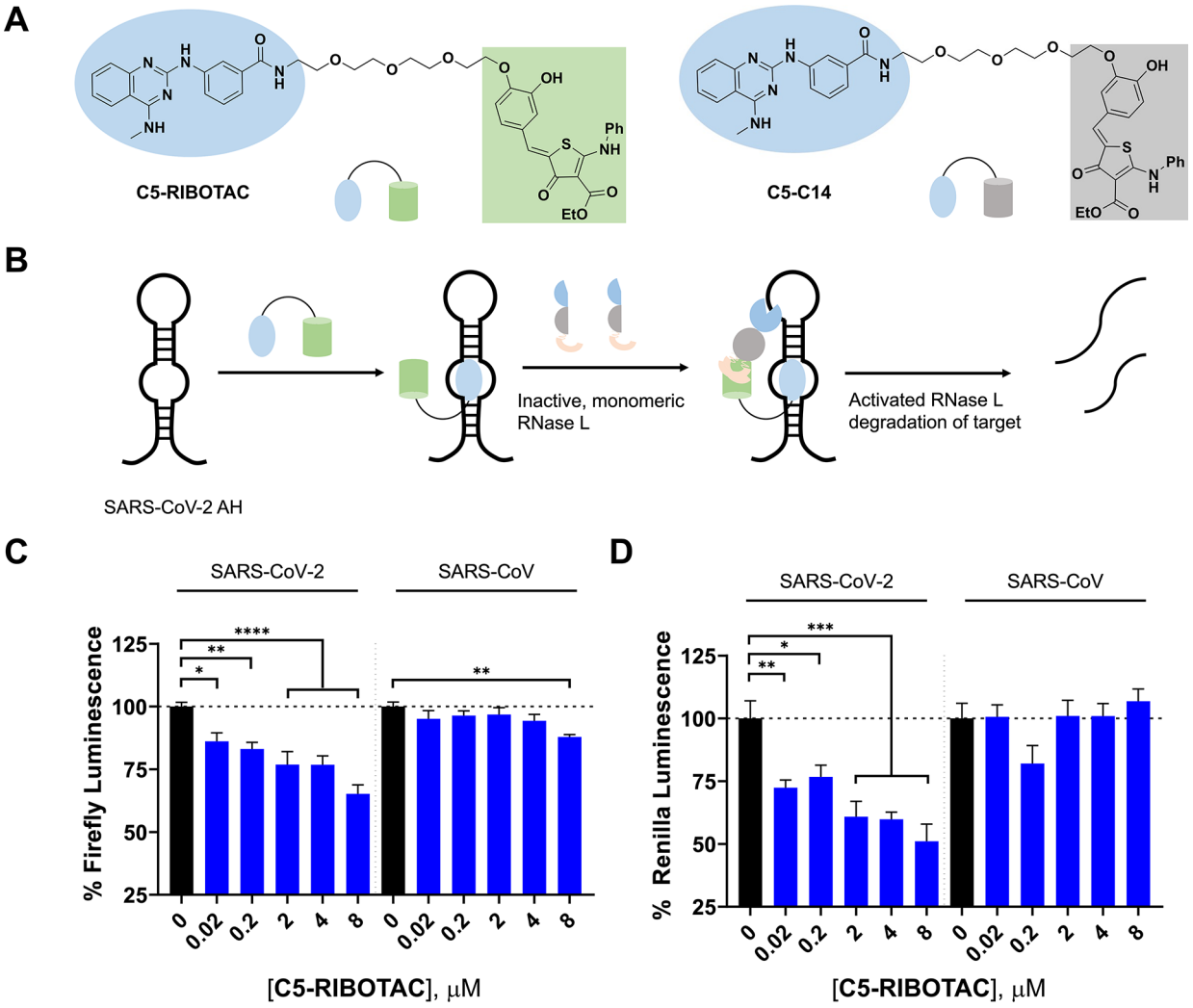

Figure 4. C5-RIBOTAC specifically degrades the SARS-CoV-2 FSE in cells. (A) Chemical structure of **C5-RIBOTAC**. The **C5** binding module is shown in blue, while the heterocyclic recruiter of RNase L is shown in green. **C5−C14** is a less active control compound in which **C5** is conjugated to a heterocycle that does not efficiently recruit RNase L. (B) Schematic of **C5-RIBOTAC** degradation of the SARS-CoV-2 RNA. **C5-RIBOTAC** recruits RNase L, dimerizing and activating it to cleave the target specifically. (C, D) Effect of **C5-RIBOTAC** on firefly (C) and Renilla (D) luciferase activities in HEK293T cells expressing the SARS-CoV-2 FSE or SARS-CoV FSE ($n = 6$ for panel C; $n = 7$ for panel D). Data are reported as the mean ± S.E.M. All p-values were calculated using a two-tailed Student t test, where *, $p < 0.05$; **, $p < 0.01$; and ***, $p < 0.001$.

ones that exceed the biologically active concentration (Figure S2B).

Further, **C5** did not affect SARS-CoV-2 FSE RNA levels, as determined by RT-qPCR (Figure 2D), nor did it have any effect on the frameshifting ability of a SARS-CoV FSE (Figure S2C−D). The SARS-CoV FSE is structurally distinct from SARS-CoV-2 and lacks the 1 × 1 nucleotide UU internal loop (Figures 1A and S1A). Collectively, these data indicate that **C5** selectively binds the internal loop to inhibit frameshifting. Notably, complete inhibition of frameshifting is likely not required to reduce viral replication. In SARS-CoV, reducing the amount of protein produced by the −1 frameshift, quantified as a percentage of the protein produced from in-frame ORF, from ∼15% (wild type) to ∼5% (afforded by mutation) almost completed ablated viral propagation and reduced viral infectivity by >3.5 orders of magnitude.[29] Thus, these molecules could have a significant effect on the virus.

Compound C5 Avidly Binds the SARS-CoV-2 AH and Increases Thermostability. To gain insight into **C5**'s mode of action, we measured its binding affinity for and thermal stabilization of the SARS-CoV-2 AH. Compound **C5** bound the UU internal loop with a K_d of 11 ± 3.8 nM (Figures S3A and S4). Binding affinity was ablated when the internal loop was switched to a base pair (no saturable binding was observed up to the greatest concentration tested, 10 μM) (Figures S3A and S4). Further, no binding was observed in a model of the SARS-CoV-AH which has a G-bulge in the stem instead of a UU internal loop (Figures S1A, S3A, and S4), in accordance with **C5**'s inability to inhibit its frameshifting (Figure S2A−C).

To determine if this avid binding confers stabilization of the AH structure, optical melting experiments were completed. Upon addition of **C5**, the $\Delta G^{\circ}_{37\,^{\circ}C}$ decreased by ∼15%, corresponding to a 1.6-fold change in its equilibrium constant at physiological temperature, suggesting that stabilization of the attenuator hairpin by **C5** contributes to the observed decrease in frameshifting efficiency. This modest change in thermodynamic stability could explain the difference in **C5**'s binding affinity and its bioactivity. Other possible reasons for this difference include (i) the target's occupancy in cells, influenced by its expression level (note the forced expression of

https://dx.doi.org/10.1021/acscentsci.0c00984
ACS Cent. Sci. XXXX, XXX, XXX−XXX

the FSE from a plasmid in these studies); (ii) cellular permeability, i.e., internal concentration; (iii) cellular localization to the cytoplasm where translation occurs; (iv) complexity of the cellular milieu versus *in vitro* binding conditions, including the target being bound by cellular proteins or being actively translated by ribosomes; and (v) binding to off-targets. Our direct target engagement studies below indicate that **C5** directly engages SARS-CoV-2 and does not bind highly expressed host mRNAs.

Cellular Target Validation via Chemical Cross-Linking and Isolation by Pull-Down (Chem-CLIP). We previously developed a target validation method dubbed Chemical Cross-Linking and Isolation by Pull-down (Chem-CLIP), a proximity-based reaction that covalently links an RNA-binding small molecule to its target(s).[30,31] We first identified a position within **C5** that could be modified with a cross-linking module without affecting its binding capacity. Modification of the carboxylic acid moiety to a propyl amide afforded a derivative dubbed **C5-PA** that has similar affinity and potency for reducing frameshifting as **C5** (Figure S3A,B). Further, **C5-PA** did not affect SARS-CoV-2 FSE mRNA levels (Figure S3C), SARS-CoV FSE frameshifting efficiency (Figure S3D), or SARS-CoV RNA levels (Figure S3E). Collectively, these data indicate that the carboxylic acid moiety is suitable for functionalization without diminishing its target engagement or specificity for the 1×1 nucleotide UU internal loop.

A **C5** derivative, dubbed **C5-Chem-CLIP**, capable of cross-linking to the FSE was afforded by appending chlorambucil as a reactive module and biotin as a purification module via **C5**'s carboxylic acid (Figure 3A). Here, the RNA-binding module drives molecular recognition, bringing chlorambucil into close proximity to the target such that they react. We first studied direct target engagement of the SARS-CoV-2 FSE by **C5-Chem-CLIP** in cells and compared it to engagement of the SARS-CoV FSE. Indeed, **C5-Chem-CLIP** directly engaged the SARS-CoV-2's RNA, which was enriched by 3-fold in the pulled down fraction as compared to the starting cell lysate (Figure 3B). In contrast, **C5-Chem-CLIP** did not enrich the SARS-CoV RNA, as expected since it lacks the small molecule's binding site (Figure 3B). Competitive (C−)Chem-CLIP studies in which cells were co-treated with a constant concentration of **C5-Chem-CLIP** and increasing concentrations of **C5** confirmed the two compounds compete for the same binding site, as a dose-dependent reduction of enrichment was observed (Figure 3C). As expected, **C5-Chem-CLIP** dose dependently reduced frameshifting in cells expressing the SARS-CoV-2 FSE, with no significant effect on frameshifting for the SARS-CoV construct (Figure S5).

To further assess selectivity, we studied whether other highly expressed mRNAs expressed by the host cell (Table S1), i.e., transcripts in HEK293T cells, were pulled down by **C5-Chem-CLIP** (n = 50). Indeed, none of these highly expressed mRNAs was bound by **C5-Chem-CLIP** (Figure 3D), confirming that the molecule is selective.

Enhancing C5 Potency: Targeted Cleavage via a Ribonuclease Targeting Chimera (RIBOTAC). Previous studies have shown that compound potency and selectivity can be enhanced in a facile fashion by converting simple binding small molecules, such as **C5**, into compounds that recruit endogenous nucleases to cleave the target catalytically and substoichiometrically, or ribonuclease targeting chimeras (RIBOTACs).[31−34] We therefore assessed whether targeted degradation of the SARS-CoV-2 RNA could increase **C5**'s potency by equipping the RNA binder with a heterocyclic RNase L-recruiting molecule[32] (via the carboxylic acid moiety), affording **C5-RIBOTAC** (Figures 4A,B). Interestingly, RNase L is part of the innate antiviral immune response, and as such, targeted degradation via a RIBOTAC could be viewed as stimulation of a *local* immune response to rid the cell of an RNA.[35,36] We also synthesized a control RIBOTAC probe in which **C5** was conjugated to a heterocycle that has a diminished ability to recruit RNase L relative to **C5-RIBOTAC**, or **C5−C14** (Figure 4A).[32] Notably, neither compound affected viability up to the highest concentration tested, in each case higher than the concentration required for bioactivity (Figure S5A).

In contrast to simple binding, **C5-RIBOTAC**'s mode of action is not stabilization of the FSE to inhibit frameshifting but targeted cleavage and degradation of the entire SARS-CoV-2 RNA. Thus, in our reporter assays, we expect degradation of the SARS-CoV-2 RNA by **C5-RIBOTAC** to result in the reduced expression of both Renilla and firefly luciferases. Indeed, dose-dependent reduction of both firefly and Renilla luciferase activity was observed upon **C5-RIBOTAC** treatment (Figure 4C,D). This reduced activity can be traced to the RIBOTAC's mode of action, as **C5-RIBOTAC** also reduced SARS-CoV-2 RNA levels dose-dependently (Figure S6A). To verify that the reduction of SARS-CoV-2 RNA levels is RNase L-dependent, we knocked down the ribonuclease with an siRNA (Figure S6B), which reduced **C5-RIBOTAC**'s activity, as assessed by measuring firefly luciferase activity (Figure S6C) and SARS-CoV-2 RNA levels (Figure S6D). No effect on compound activity was observed with a control, scrambled siRNA (Figure S6C,D). In contrast, **C5-RIBOTAC** had no significant effect on the luminescence signals, whether firefly or Renilla, generated from HEK293T cells expressing the SARS-CoV construct (Figure 4C,D) or on SARS-CoV RNA levels (Figure S6A).

As expected, the less active RIBOTAC, **C5−C14**, reduced frameshifting efficiency of the SARS CoV-2 FSE (with modestly reduced potency compared to **C5**), as the RNA-binding module (**C5**) maintains its ability to bind its target (Figure S7A). In agreement with a simple binding, not cleavage, mode of action, **C5−C14** had no effect on SARS-CoV-2 RNA levels (Figure S7B). Compound **C5−C14**'s modestly reduced potency could be due to differences in cellular permeability as **C5−C14** and **C5** bind the SARS-CoV-2 FSE with similar affinity (Figure S4A). The control RIBOTAC also had no effect on the frameshifting efficiency, or the RNA levels of the SARS-CoV construct, as expected (Figure S7B−C).

It is difficult to compare directly the enhancement in potency due to nuclease recruitment vs simple binding, i.e., **C5** versus **C5-RIBOTAC**, because the readout of activity is different. If we compare the concentration of **C5** required to reduce frameshifting efficiency by ∼25% (2 μM; Figure 2C) to the concentration **C5-RIBOTAC** required to reduce Renilla luciferase activity by ∼25% (0.2 μM; Figure 4D), then nuclease recruitment affords an ∼10-fold increase in potency. If only the effect of each compound on firefly luciferase activity is considered, then an ∼100-fold increase in potency is observed (Figure S7D). This enhancement is similar to those observed for RIBOTACs that target other RNAs for degradation[32−34,37] as well as those observed for proteolysis targeting chimeras (PROTACs; 10−500-fold).[38]

https://dx.doi.org/10.1021/acscentsci.0c00984
ACS Cent. Sci. XXXX, XXX, XXX−XXX

We previously reported a simple binding compound and its RIBOTAC that selectively inactivate the miR-17/92 cluster that encodes six mature microRNAs. Interestingly, conversion of this ligand into a RIBOTAC altered the small molecule's cellular localization, rendering it primarily to the cytoplasm where RNase L is also located.[37] As the replication of (+)RNA viruses, like SARS-CoV-2, occurs in the cytoplasm, they, as well as mRNAs in general, are well suited as targets for RIBOTACs.[39,40]

CONCLUSIONS

The scientific community is pursuing multiple strategies to address the ongoing SARS-CoV-2 pandemic, from vaccine development to drug repurposing and discovery. On the basis of the most recent structural studies, revealing robust structures in the virus' genome, we tested the druggability of the SARS-CoV-2's frameshifting element. Using AbsorbArray and luciferase reporter-based cellular assays, we identified a hit compound, **C5**, that selectively binds to and stabilizes the attenuator hairpin of the FSE, reducing its frameshifting efficiency in cells. Interestingly, **C1** and **C3** modulated frameshifting to a slightly greater extent than **C5**, enhancing translation of the in-frame ORF (Figure 2B), and are currently the subject of further evaluation. We further elaborated **C5** into a covalent binder (**C5-Chem-CLIP**) and an RNA degrader (**C5-RIBOTAC**) to validate target engagement and to enhance potency via targeted degradation of the viral RNA, respectively.

Our results demonstrated that small molecules can selectively bind to the FSE of SARS-CoV-2 and impede its function in cells. Although the compounds will need to be further studied and developed for affecting live virus, these studies support the hypothesis that the SARS-CoV-2 genome could be a reservoir of potential drug targets that can be affected quickly by using RNA structure-targeting ligands. While much more effort is needed for drug development, our study suggests that small molecules can indeed engage a functional site within the SARS-CoV-2 genome and disrupt its cellular function. As studies have emerged on investigating the structure of the entire SARS-CoV-2 genome, there are likely to be other sites that can be targeted to affect the virus. These sites can be interrogated efficiently by using structure-specific ligands designed from sequence by Inforna[26] and RIBOTACs, which importantly do not require binding to a functional site.[32]

ASSOCIATED CONTENT

Supporting Information

The Supporting Information is available free of charge at https://pubs.acs.org/doi/10.1021/acscentsci.0c00984.

(i) Supporting Table 1; (ii) Supporting Figures 1−7; (iii) Experimental Methods; and (iv) compound characterization (PDF)

AUTHOR INFORMATION

Corresponding Author

Matthew D. Disney − *The Scripps Research Institute, Department of Chemistry, Jupiter, Florida 33458, United States;* orcid.org/0000-0001-8486-1796; Email: disney@scripps.edu

Authors

Hafeez S. Haniff − *The Scripps Research Institute, Department of Chemistry, Jupiter, Florida 33458, United States;* orcid.org/0000-0002-5561-5251

Yuquan Tong − *The Scripps Research Institute, Department of Chemistry, Jupiter, Florida 33458, United States*

Xiaohui Liu − *The Scripps Research Institute, Department of Chemistry, Jupiter, Florida 33458, United States*

Jonathan L. Chen − *The Scripps Research Institute, Department of Chemistry, Jupiter, Florida 33458, United States;* orcid.org/0000-0001-7907-9732

Blessy M. Suresh − *The Scripps Research Institute, Department of Chemistry, Jupiter, Florida 33458, United States*

Ryan J. Andrews − *Roy J. Carver Department of Biophysics, Biochemistry and Molecular Biology, Iowa State University, Ames, Iowa 50011, United States;* orcid.org/0000-0003-0275-0019

Jake M. Peterson − *Roy J. Carver Department of Biophysics, Biochemistry and Molecular Biology, Iowa State University, Ames, Iowa 50011, United States*

Collin A. O'Leary − *Roy J. Carver Department of Biophysics, Biochemistry and Molecular Biology, Iowa State University, Ames, Iowa 50011, United States*

Raphael I. Benhamou − *The Scripps Research Institute, Department of Chemistry, Jupiter, Florida 33458, United States;* orcid.org/0000-0003-1743-0886

Walter N. Moss − *Roy J. Carver Department of Biophysics, Biochemistry and Molecular Biology, Iowa State University, Ames, Iowa 50011, United States*

Complete contact information is available at: https://pubs.acs.org/10.1021/acscentsci.0c00984

Author Contributions

#H.S.H. and Y.T. contributed equally.

Notes

The authors declare the following competing financial interest(s): Matthew D. Disney is a founder of Expansion Therapeutics.

Data Availability. All associated raw data that support the findings of this study are available from the corresponding author upon reasonable request.

ACKNOWLEDGMENTS

This work was funded by the National Institutes of Health (R01 CA249180, and R35 NS116846 to M.D.D; as well as NIH/NIGMS Grants R00 GM112877 and R01 GM133810 to W.N.M). We thank Dr. Jessica Childs-Disney for assistance with writing and editing the manuscript and Prof. Jonathan D. Dinman at the University of Maryland College Park for providing the SARS-CoV-2, SARS-CoV, and ORF reporter plasmids used in these studies.

REFERENCES

(1) Schröder, I. COVID-19: A risk assessment perspective. *ACS Chem. Health Saf.* **2020**, *27* (3), 160.

(2) Ivanov, D. Predicting the impacts of epidemic outbreaks on global supply chains: A simulation-based analysis on the coronavirus outbreak (COVID-19/SARS-CoV-2) case. *Transp. Res. E Logist. Transp. Rev.* **2020**, *136*, 101922−101936.

(3) Zhang, Y.-Z.; Holmes, E. C. A genomic perspective on the origin and emergence of SARS-CoV-2. *Cell* **2020**, *181* (2), 223−227.

(4) Amanat, F.; Krammer, F. SARS-CoV-2 vaccines: status report. *Immunity* **2020**, *52* (4), 583−589.

(5) Zhang, T.; Wu, Q.; Zhang, Z. Probable pangolin origin of SARS-CoV-2 associated with the COVID-19 outbreak. *Curr. Biol.* **2020**, *30* (7), 1346−1351.
(6) Wang, M.; Cao, R.; Zhang, L.; Yang, X.; Liu, J.; Xu, M.; Shi, Z.; Hu, Z.; Zhong, W.; Xiao, G. Remdesivir and chloroquine effectively inhibit the recently emerged novel coronavirus (2019-nCoV) in vitro. *Cell Res.* **2020**, *30* (3), 269−271.
(7) Agostini, M. L.; Andres, E. L.; Sims, A. C.; Graham, R. L.; Sheahan, T. P.; Lu, X.; Smith, E. C.; Case, J. B.; Feng, J. Y.; Jordan, R.; Ray, A. S.; Cihlar, T.; Siegel, D.; Mackman, R. L.; Clarke, M. O.; Baric, R. S.; Denison, M. R. Coronavirus susceptibility to the antiviral remdesivir (GS-5734) Is mediated by the viral polymerase and the proofreading exoribonuclease. *mBio* **2018**, *9* (2), 1−15.
(8) Zhang, G.; Pomplun, S.; Loftis, A. R.; Tan, X.; Loas, A.; Pentelute, B. L. Investigation of ACE2 N-terminal fragments binding to SARS-CoV-2 Spike RBD. *bioRxiv* **2020**, 2020.03.19.999318.
(9) Gordon, D. E.; Jang, G. M.; Bouhaddou, M.; Xu, J.; Obernier, K.; White, K. M.; O'Meara, M. J.; Rezelj, V. V.; Guo, J. Z.; Swaney, D. L.; Tummino, T. A.; Huettenhain, R.; Kaake, R. M.; Richards, A. L.; Tutuncuoglu, B.; Foussard, H.; Batra, J.; Haas, K.; Modak, M.; Kim, M.; Haas, P.; Polacco, B. J.; Braberg, H.; Fabius, J. M.; Eckhardt, M.; Soucheray, M.; Bennett, M. J.; Cakir, M.; McGregor, M. J.; Li, Q.; Meyer, B.; Roesch, F.; Vallet, T.; Mac Kain, A.; Miorin, L.; Moreno, E.; Naing, Z. Z. C.; Zhou, Y.; Peng, S.; Shi, Y.; Zhang, Z.; Shen, W.; Kirby, I. T.; Melnyk, J. E.; Chorba, J. S.; Lou, K.; Dai, S. A.; Barrio-Hernandez, I.; Memon, D.; Hernandez-Armenta, C.; Lyu, J.; Mathy, C. J. P.; Perica, T.; Pilla, K. B.; Ganesan, S. J.; Saltzberg, D. J.; Rakesh, R.; Liu, X.; Rosenthal, S. B.; Calviello, L.; Venkataramanan, S.; Liboy-Lugo, J.; Lin, Y.; Huang, X. P.; Liu, Y.; Wankowicz, S. A.; Bohn, M.; Safari, M.; Ugur, F. S.; Koh, C.; Savar, N. S.; Tran, Q. D.; Shengjuler, D.; Fletcher, S. J.; O'Neal, M. C.; Cai, Y.; Chang, J. C. J.; Broadhurst, D. J.; Klippsten, S.; Sharp, P. P.; Wenzell, N. A.; Kuzuoglu-Ozturk, D.; Wang, H. Y.; Trenker, R.; Young, J. M.; Cavero, D. A.; Hiatt, J.; Roth, T. L.; Rathore, U.; Subramanian, A.; Noack, J.; Hubert, M.; Stroud, R. M.; Frankel, A. D.; Rosenberg, O. S.; Verba, K. A.; Agard, D. A.; Ott, M.; Emerman, M.; Jura, N.; von Zastrow, M.; Verdin, E.; Ashworth, A.; Schwartz, O.; d'Enfert, C.; Mukherjee, S.; Jacobson, M.; Malik, H. S.; Fujimori, D. G.; Ideker, T.; Craik, C. S.; Floor, S. N.; Fraser, J. S.; Gross, J. D.; Sali, A.; Roth, B. L.; Ruggero, D.; Taunton, J.; Kortemme, T.; Beltrao, P.; Vignuzzi, M.; Garcia-Sastre, A.; Shokat, K. M.; Shoichet, B. K.; Krogan, N. J. A SARS-CoV-2 protein interaction map reveals targets for drug repurposing. *Nature* **2020**, *583*, 459−488.
(10) Lan, T. C. T.; Allan, M. F.; Malsick, L. E.; Khandwala, S.; Nyeo, S. S. Y.; Bathe, M.; Griffiths, A.; Rouskin, S. Structure of the full SARS-CoV-2 RNA genome in infected cells. *bioRxiv* **2020**, 2020.06.29.178343.
(11) Rangan, R.; Zheludev, I. N.; Das, R. RNA genome conservation and secondary structure in SARS-CoV-2 and SARS-related viruses. *bioRxiv* **2020**, 2020.03.27.012906.
(12) Andrews, R. J.; Peterson, J. M.; Haniff, H. S.; Chen, J.; Williams, C.; Grefe, M.; Disney, M. D.; Moss, W. N. An in silico map of the SARS-CoV-2 RNA structurome. *bioRxiv* **2020**, 2020.04.17.045161.
(13) Blanco-Melo, D.; Nilsson-Payant, B. E.; Uhl, S.; Escudero-Pèrez, B.; Olschewski, S.; Thibault, P.; Panis, M.; Rosenthal, M.; Muñoz-Fontela, C.; Lee, B.; tenOever, B. R. An inability to maintain the ribonucleoprotein genomic structure is responsible for host detection of negative-sense RNA viruses. *bioRxiv* **2020**, 2020.03.12.989319.
(14) Disney, M. D. Targeting RNA with small molecules to capture opportunities at the intersection of chemistry, biology, and medicine. *J. Am. Chem. Soc.* **2019**, *141* (17), 6776−6790.
(15) Costales, M. G., Childs-Disney, J. L., Disney, M. D. Computational tools for design of selective small molecules targeting RNA: from small molecule microarrays to chemical similarity searching. Garner, A., Eds.; In *RNA Therapeutics. Topics in Medicinal Chemistry*; Springer, Cham., 2017; Vol 27. DOI: 10.1007/7355_2016_21.
(16) Hermann, T. Small molecules targeting viral RNA. *WIREs RNA* **2016**, *7* (6), 726−743.
(17) Park, S.-J.; Kim, Y.-G.; Park, H.-J. Identification of RNA pseudoknot-binding ligand that inhibits the −1 ribosomal frameshifting of SARS-coronavirus by structure-based virtual screening. *J. Am. Chem. Soc.* **2011**, *133* (26), 10094−10100.
(18) Kelly, J. A.; Olson, A. N.; Neupane, K.; Munshi, S.; San Emeterio, J.; Pollack, L.; Woodside, M. T.; Dinman, J. D. Structural and functional conservation of the programmed −1 ribosomal frameshift signal of SARS coronavirus 2 (SARS-CoV-2). *bioRxiv* **2020**, 2020.03.13.991083.
(19) Tan, Y.-J.; Lim, S. G.; Hong, W. Characterization of viral proteins encoded by the SARS-coronavirus genome. *Antiviral Res.* **2005**, *65* (2), 69−78.
(20) Graham, R. L.; Sparks, J. S.; Eckerle, L. D.; Sims, A. C.; Denison, M. R. SARS coronavirus replicase proteins in pathogenesis. *Virus Res.* **2008**, *133* (1), 88−100.
(21) Cho, C. P.; Lin, S. C.; Chou, M. Y.; Hsu, H. T.; Chang, K. Y. Regulation of programmed ribosomal frameshifting by co-translational refolding RNA hairpins. *PLoS One* **2013**, *8* (4), No. e62283.
(22) Su, M.-C.; Chang, C.-T.; Chu, C.-H.; Tsai, C.-H.; Chang, K.-Y. An atypical RNA pseudoknot stimulator and an upstream attenuation signal for −1 ribosomal frameshifting of SARS coronavirus. *Nucleic Acids Res.* **2005**, *33* (13), 4265−4275.
(23) Lan, T. C. T.; Allan, M. F.; Malsick, L.; Khandwala, S.; Nyeo, S. S. Y.; Bathe, M.; Griffiths, A.; Rouskin, S. Structure of the full SARS-CoV-2 RNA genome in infected cells. *bioRxiv* **2020**, 2020.06.29.178343.
(24) Hu, H. T.; Cho, C. P.; Lin, Y. H.; Chang, K. Y. A general strategy to inhibiting viral −1 frameshifting based on upstream attenuation duplex formation. *Nucleic Acids Res.* **2016**, *44* (1), 256−66.
(25) Ofori, L. O.; Hilimire, T. A.; Bennett, R. P.; Brown, N. W., Jr.; Smith, H. C.; Miller, B. L. High-affinity recognition of HIV-1 frameshift-stimulating RNA alters frameshifting in vitro and interferes with HIV-1 infectivity. *J. Med. Chem.* **2014**, *57* (3), 723−32.
(26) Velagapudi, S. P.; Gallo, S. M.; Disney, M. D. Sequence-based design of bioactive small molecules that target precursor microRNAs. *Nat. Chem. Biol.* **2014**, *10* (4), 291−297.
(27) Hafeez, H.; Laurent, K.; Xiaohui, L.; Gogce, C.; Jonas, B.; Daniel, A.; Alexander, A.; Malin, L.; Matthew, D., Design of a small molecule that stimulates VEGFA enabled by screening RNA fold-small molecule interactions. *Nat. Chem.* **2020**, DOI: 10.1038/s41557-020-0514-4.
(28) Velagapudi, S. P.; Costales, M. G.; Vummidi, B. R.; Nakai, Y.; Angelbello, A. J.; Tran, T.; Haniff, H. S.; Matsumoto, Y.; Wang, Z. F.; Chatterjee, A. K.; Childs-Disney, J. L.; Disney, M. D. Approved anti-cancer drugs target oncogenic non-coding RNAs. *Cell Chem. Biol.* **2018**, *25* (9), 1086−1094.
(29) Plant, E. P.; Rakauskaite, R.; Taylor, D. R.; Dinman, J. D. Achieving a golden mean: mechanisms by which coronaviruses ensure synthesis of the correct stoichiometric ratios of viral proteins. *J. Virol.* **2010**, *84* (9), 4330−4340.
(30) Velagapudi, S. P.; Li, Y.; Disney, M. D. A cross-linking approach to map small molecule-RNA binding sites in cells. *Bioorg. Med. Chem. Lett.* **2019**, *29* (12), 1532−1536.
(31) Rzuczek, S. G.; Colgan, L. A.; Nakai, Y.; Cameron, M. D.; Furling, D.; Yasuda, R.; Disney, M. D. Precise small-molecule recognition of a toxic CUG RNA repeat expansion. *Nat. Chem. Biol.* **2017**, *13* (2), 188−193.
(32) Costales, M. G.; Aikawa, H.; Li, Y.; Childs-Disney, J. L.; Abegg, D.; Hoch, D. G.; Pradeep Velagapudi, S.; Nakai, Y.; Khan, T.; Wang, K. W.; Yildirim, I.; Adibekian, A.; Wang, E. T.; Disney, M. D. Small-molecule targeted recruitment of a nuclease to cleave an oncogenic RNA in a mouse model of metastatic cancer. *Proc. Natl. Acad. Sci. U. S. A.* **2020**, *117* (5), 2406−2411.
(33) Costales, M. G.; Matsumoto, Y.; Velagapudi, S. P.; Disney, M. D. Small molecule targeted recruitment of a nuclease to RNA. *J. Am. Chem. Soc.* **2018**, *140* (22), 6741−6744.

https://dx.doi.org/10.1021/acscentsci.0c00984
ACS Cent. Sci. XXXX, XXX, XXX−XXX

(34) Costales, M. G.; Suresh, B.; Vishnu, K.; Disney, M. D. Targeted degradation of a hypoxia-associated non-coding RNA enhances the selectivity of a small molecule interacting with RNA. *Cell Chem. Biol.* **2019**, *26* (8), 1180−1186.
(35) Wreschner, D. H.; McCauley, J. W.; Skehel, J. J.; Kerr, I. M. Interferon action–sequence specificity of the ppp(A2′p)$_n$A-dependent ribonuclease. *Nature* **1981**, *289* (5796), 414−7.
(36) Floyd-Smith, G.; Slattery, E.; Lengyel, P. Interferon action: RNA cleavage pattern of a (2′-5′)oligoadenylate–dependent endonuclease. *Science* **1981**, *212* (4498), 1030−2.
(37) Liu, X.; Haniff, H. S.; Childs-Disney, J. L.; Shuster, A.; Aikawa, H.; Adibekian, A.; Disney, M. D. Targeted degradation of the oncogenic microRNA 17−92 cluster by structure-targeting ligands. *J. Am. Chem. Soc.* **2020**, *142* (15), 6970−6982.
(38) Ottis, P.; Crews, C. M. Proteolysis-targeting chimeras: induced protein degradation as a therapeutic strategy. *ACS Chem. Biol.* **2017**, *12* (4), 892−898.
(39) Tao, Y. J.; Ye, Q. RNA virus replication complexes. *PLoS Pathog.* **2010**, *6* (7), No. e1000943.
(40) Fehr, A. R.; Perlman, S. Coronaviruses: an overview of their replication and pathogenesis. *Methods Mol. Biol.* **2015**, *1282*, 1−23.

https://dx.doi.org/10.1021/acscentsci.0c00984
ACS Cent. Sci. XXXX, XXX, XXX−XXX